



City Research Online

City, University of London Institutional Repository

Citation: Bobba, S. S. & Agrawal, A. (2017). Ultra-broad Mid-IR Supercontinuum Generation in Single, Bi and Tri Layer Graphene Nano-Plasmonic waveguides pumping at Low Input Peak Powers. Scientific Reports, 7(1), 10192.. doi: 10.1038/s41598-017-10141-3

This is the published version of the paper.

This version of the publication may differ from the final published version.

Permanent repository link: <http://openaccess.city.ac.uk/18118/>

Link to published version: <http://dx.doi.org/10.1038/s41598-017-10141-3>

Copyright and reuse: City Research Online aims to make research outputs of City, University of London available to a wider audience. Copyright and Moral Rights remain with the author(s) and/or copyright holders. URLs from City Research Online may be freely distributed and linked to.

City Research Online:

<http://openaccess.city.ac.uk/>

publications@city.ac.uk

SCIENTIFIC REPORTS



OPEN

Ultra-broad Mid-IR Supercontinuum Generation in Single, Bi and Tri Layer Graphene Nano-Plasmonic waveguides pumping at Low Input Peak Powers

Swetha S. Bobba & Arti Agrawal

This article presents four different plasmonic structures using Graphene which yielded an efficient plasmonic mode with low loss for Supercontinuum(SC) generation. At an operating wavelength of 1550 nm in these structures, we generated a multi-octave broadband SC spectrum ranging from 1.5 μm –25 μm at a low input peak power of 1W. Due to pumping in the anomalous dispersion region with two Zero Dispersion Wavelengths (ZDWs) and the process of cross phase modulation with soliton fission, red-shifted dispersive waves were generated which led to large broadening from 1.5 μm –25 μm . Two other Supercontinua ranging from 1–10 μm and 0.85–2.2 μm also at low input peak powers of 2W and 0.1W respectively were generated. These three supercontinua are useful for applications in the fields of biomedical sensors, spectroscopy, fluorescence lifetime imaging and in the design of many other new optical devices. Furthermore, we have also discussed our results on behaviour of Graphene as a metal, even without the negative real value of dielectric constant.

Supercontinuum Generation (SCG) has been widely studied over the past 40 years. Detailed analysis of non-linear dynamics in solids, organic and inorganic liquids, gases¹, various types of waveguides and optical fibres^{2,3} has led to the design of wide-band Supercontinuum light sources. However, they require very high input peak powers ranging from 1 kW to 1000 kW or more²⁻⁹. From the literature in the area¹⁰⁻¹³, low input peak powers (of the order of Watts) has limited the spectral broadening and thereby their usability for wide range of applications¹⁴. Dispersion engineered waveguides and/or fibres using different materials have been developed but their main limitation is the control of peak input power with low loss for broadband SCG.

For example, in 2015, Yu *et al.* generated a SC spanning from 1.8 to 10 μm by pumping a Ge-As-Se/Ge-As-S chalcogenide fibre with 330 fs pulses at 4 μm using ~ 3000 W input³. In 2016, a three-layer index guided lead silicate (SF57) photonic crystal fibre⁴ was used to generate three octaves spanning SC from 900 to 7200 nm using 50 fs sech optical pulses of 5 kW peak input power with a large nonlinear coefficient of ~ 1078 W⁻¹ km⁻¹. Recently, Cheng *et al.* experimentally demonstrated mid-infrared (MIR) SCG spanning ~ 2.0 to 15.1 μm in a 3 cm-long chalcogenide step-index fiber with a pulse width of ~ 170 fs at 9.8 μm with input peak power of 2.89 MW⁵. This is the highest average power SC covering 2–15.1 μm reported to date. Also, the broadening beyond 15 μm for this design is not possible due to material absorption of the chalcogenide. Our results thus emphasize on solutions to these problems – the peak input power and loss by using Graphene as one of the core materials for the waveguide designs.

Graphene¹⁵ is a two-dimensional (2D) Carbon material with a honey-comb lattice. Recently Graphene nano-ribbon and other waveguides have emerged showing possible outstanding applications in the fields of on-chip interconnects, bright visible light emission, flexible electronics and more^{16,17}. However, in all these designs, Graphene has been used as the outer core or the cladding material. Thus, from our research, we have shown that with Graphene as the inner core in the designed waveguides, we can exploit its remarkable non-linear

Department of Electrical and Electronic Engineering, City, University of London, Northampton Square, London, EC1V 0HB, UK. Correspondence and requests for materials should be addressed to A.A. (email: arti.agrawal.1@city.ac.uk)

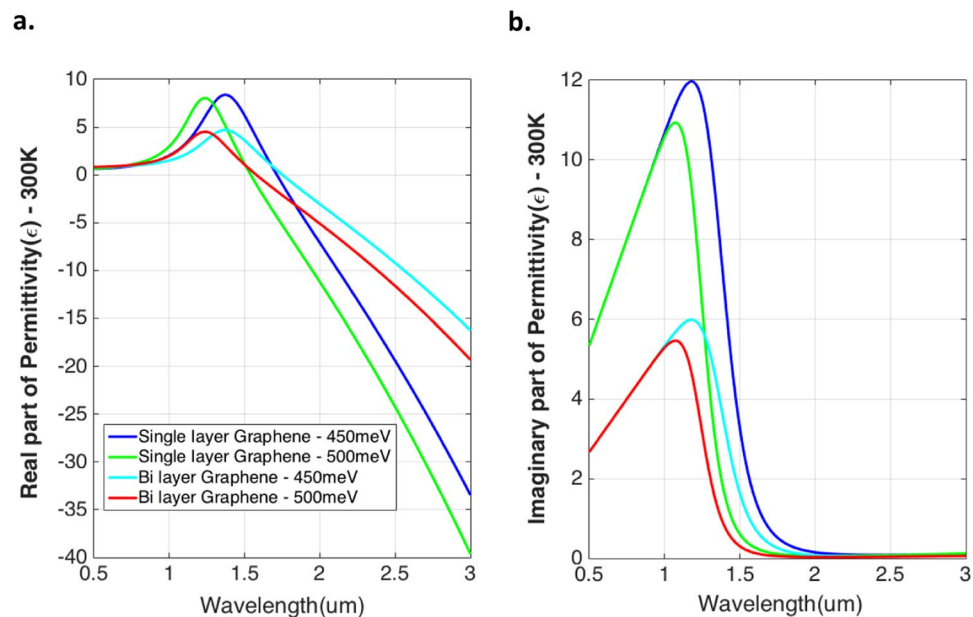


Figure 1. Real and Imaginary part of Permittivity of Graphene plotted from 0.5–3 μm . (a,b), Calculated permittivity of Graphene at two different chemical potentials and temperatures of 450 meV and 500 meV at 300 K. These results are benchmarked with [50].

Temperature (T)	Chemical Potential (μ_c)	Operating Wavelength (λ)	σ_g (Conductivity of Graphene)	ϵ_g (Permittivity)
300 K	450 meV	1.55 μm	$7.78289151434 \times 10^{-06} - 1.322691198868 \times 10^{-05} \text{ S}$	$4.6233 + 2.1320i$
371 K	450 meV	1.55 μm	$1.05877013296 \times 10^{-05} - 1.231768904974 \times 10^{-05} \text{ S}$	$4.3742 + 2.9003i$
300 K	500 meV	1.55 μm	$1.3906881552 \times 10^{-06} + 4.9808553475 \times 10^{-06} \text{ S}$	$-0.3644 + 0.3810i$
371 K	500 meV	1.55 μm	$2.685510752162 \times 10^{-06} + 4.204475290258 \times 10^{-06} \text{ S}$	$-0.1517 + 0.7356i$

Table 1. Calculated conductivity and permittivity of single layer Graphene at 1550 nm for 450 meV and 500 meV - 300 K and 371 K.

properties including a very high Kerr coefficient of $-1.1 \times 10^{-13} \text{ m}^2/\text{W}^{18}$ for broadband SCG at a low input peak power, while exhibiting low material losses.

Waveguide Design and Implementation

In our design of Graphene waveguides for SCG: the structure of a ridge waveguide rests on a Silicon dioxide (SiO_2) substrate with the inner and outer core surrounded by a low-index medium (air), thereby providing strong optical confinement.

The inner core of the designed ridge waveguides consists of a single or bi layer of Graphene, of thickness 0.335 nm and 0.67 nm respectively. A material (Si_3N_4) with hexagonal crystalline structure capable of controlling the overall waveguide loss, with tunable band-gap properties for electro-optic applications is used as the outer core. This design thereby produces an efficient mode to guide the light leading to broader SC. The low refractive index contrast of the waveguide materials was kept in mind to avoid large non-linear effects which can narrow the Supercontinuum broadening with losses.

Four Graphene waveguide designs (Single, with and without buffer for Bi, and only with Buffer for Tri layers) were simulated using Finite Element Method (FEM)^{19,20} to calculate the Group Velocity Dispersion (GVD, β_2) curve and the respective higher order dispersion coefficients (β_3, β_4). Supercontinuum for these designs were further calculated by solving the Generalized Non-Linear Schrödinger Equation (GNLSE) using the Split-step Fourier method.

In all the simulations performed, Graphene was tuned to two chemical potentials, $\mu_c = 450 \text{ meV}$ and 500 meV , which can be achieved by applying a gate voltage to the 2D material. This range of chemical potentials were specifically used to tune Graphene as a metal in the operating wavelength region (1550 nm) with low waveguide loss, thereby generating a plasmonic mode at the dielectric-metal-dielectric interface.

Results

The Conductivity (σ_g) and Permittivity (ϵ_g) of single and bi layer of Graphene were calculated from the Kubo formula^{21–23} using a FORTRAN code developed by us. The wavelength variation of the real and imaginary parts of the permittivity is shown in Fig. 1a and b, at 450 and 500 meV, 300 K. Table 1 shows these values for single layer of Graphene operating at 1550 nm wavelength (at 300 K and 371 K).

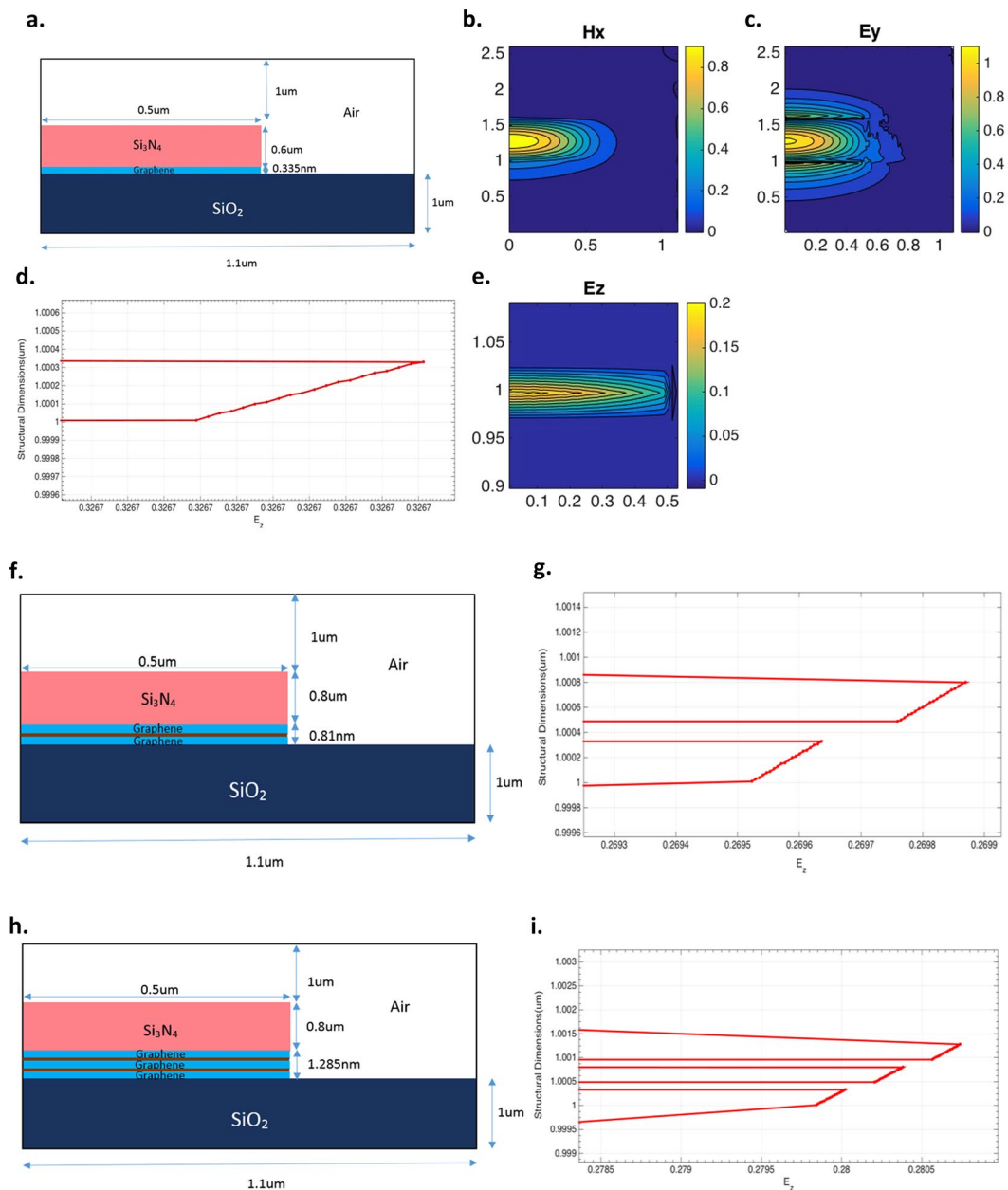


Figure 2. Plasmonic modes generated in the Graphene layer of the designed waveguides at 450 meV and 300 K. (**a–e**), Structure of the single layer Graphene Waveguide with dominant field components H_x , E_y , E_z and, plasmonic mode (line plot of E_z) on the left. (**f,h**), Bi-layer and Tri-layer Graphene waveguides sandwiched with Al_2O_3 buffer layer (region shaded brown) of thickness 0.14 nm. (**g,i**) The plasmonic modes of bi and tri layer Graphene waveguides on the right.

The waveguide with a single layer of Graphene (Fig. 2a) with complex permittivity calculated at 450 meV, 300 K (from Table 1) was used in the half-waveguide cross section of $1.1 \mu\text{m}$ wide \times $2.600335 \mu\text{m}$ height to guide the fundamental TM mode initially. The outer core - Si_3N_4 (Silicon Nitride) is used with permittivity, $\epsilon_{Si_3N_4} = 6.0945364$ on top of the Graphene layer with Silica (SiO_2), $\epsilon_{SiO_2} = 2.0852$ as the substrate, and Air, $\epsilon_{Air} = 1$ for the cladding operating at 1550 nm. Figure 2b,c and e shows the dominant H_x , E_y and E_z field components generated in this structure with the plasmonic mode shown in Fig. 2d. Numerical simulations were then extended to bi (with buffer) and tri (with buffer) layer waveguides as shown in Fig. 2f and h at a chemical potential of 450 meV and temperature of 300 K. It is apparent from the field representation in E_z and the plasmonic mode plots from Fig. 2d,g and i, that the mode is highly confined in the inner core of the designed Graphene ridge waveguides and is a plasmonic mode.

The plasmonic mode^{24,25} in Graphene layer of the designed waveguide geometries is formed from coupling between Surface Plasmon Polaritons (SPPs) generated on the top and bottom interfaces of the 2D material with Silicon Nitride and Silica layers respectively. Thickness of Graphene^{22,26} also plays a vital role in tight electric

field localization at the metal interface, thereby guiding the EM energy with sub-wavelength confinement to micron/sub-micron propagation lengths. Similar physics but with slightly different values of GVD, A_{eff} and loss was observed in these waveguide designs at 450 meV, 371 K, with plasmonic mode-shifting from z to y - axis at 500 meV–300 K and 371 K. This property makes these designs sensitive for sensor applications²⁶ that will be investigated in the future.

Figure 3a–f show the GVD curve (β_2), effective mode area (A_{eff}) and loss plots calculated at a step size of 0.025 μm from 1.5–2 μm wavelength range for all the four designed waveguide structures at 450 meV, 371 K and 500 meV, 300 K respectively. The GVD Curves²⁷ show the presence of increasing and decreasing slopes after reaching a peak dispersion value which results in two ZDWs.

At 1.55 μm , bi and tri layer graphene waveguides induced a total effective area of 0.962449 μm^2 and 0.9593657 μm^2 at 300 K, and 0.9613992 μm^2 and 0.9578994 μm^2 at 371 K, for 500 meV chemical potential. These structures also showed an average loss of only ~ 15 dB/km. The overall dispersion in bi and tri layer structures (with buffer) was moderate with excellent A_{eff} and loss, thereby making them highly [Comment: The below sentence is continuation from the above paragraph, as in, the sentence should read “thereby making them highly favourable for SCG”] favourable for SCG. Similar properties of this GVD curve in Fig. 3a and d was observed at 450 meV, 300 K and 500 meV, 371 K respectively, but with a very small difference of GVD as plotted in Fig. 3g.

SC Generation. Supercontinuum in the designed Graphene waveguides was generated operating at 1550 nm, at a pulse width of 10, 2.5 and 1fs for 1 mm, 10 μm and 1 mm long waveguides as shown in Fig. 4a,b and c respectively. This generated three Supercontinua, one with multi-octave broadband spectra ranging from 1.5 μm –25 μm (Fig. 4c) at a very low input peak power of 1 W, thereby making it the broadest Supercontinuum to the best of our knowledge at low input power of the order of 1 W. Two other Supercontinua (Fig. 4b and c) ranging from 1–10 μm and 0.85–2.2 μm also at very low input peak powers of 2 W and 0.1 W respectively were generated using these designs. Figure 4a–c show that the SC generated (at low input peak powers) in the designed Graphene waveguides exhibit flat spectral broadening (upto 20 dB).

Discussion

The broad expansion of the SC in Fig. 4c to such a large bandwidth in our design is mainly due to the large non-linear Kerr coefficient of Graphene of the order of $\sim 10^{-13}$ m^2/W . This Kerr coefficient parameter²⁸ combined with the tailored dispersion of the waveguide generated fundamental optical solitons thereby stimulating dispersive wave radiation in the anomalous dispersion region. The spectral expansion is mainly due to those successively ejected fundamental solitons from the input pulse^{29,30} during soliton fission.

The largest spectral bandwidth is observed in the Graphene Single layer structure shown in Fig. 4c. However, considering the losses calculated for the four designed waveguides shown in Fig. 3c,f, we find that the Graphene Bi layer with Buffer (at 500 meV, 300 K) structure is also an efficient waveguide design for SCG. We present further results on the dynamics of this SC^{31,32} in the following material.

For the 1 mm-long Graphene waveguide at a pulse width of 10fs, shown in Fig. 5a1, the nonlinear length is calculated using³¹ $L_{\text{NL}} = 1/(\gamma P_0)$, where γ is the nonlinear coefficient and P_0 is the peak input power. From calculations, we get L_{NL} at the 1550 nm pump wavelength as 21.584 μm . The dispersion length is $L_D = T_0^2/|\beta_2|$, where T_0 is the pulse width and $\beta_2 = -1.068446552230430$ ps^2/m at 1.55 μm is the dispersion parameter calculated from Fig. 3. For the peak input power of 0.1 W, L_{NL} is 21.584 $\times 10^{-6}$ m, and L_D is 9.3594 $\times 10^{-5}$ m. Also, the characteristic propagation distance ($\approx 5L_D$) where the ejected soliton separation begins to become apparent in the temporal and spectral characteristic is calculated as $\approx 4.6797 \times 10^{-4}$ m. Since the waveguide length $L = 1$ mm is slightly larger than $5L_D$ and is greater than both L_{NL} and L_D , the spectrum leads to a number of ejected solitons appearing with a significant decrease of spectral energy in the vicinity of the pump thereby limiting the spectral bandwidth³⁰. The soliton order(N) of the waveguide for these input parameters is calculated as ~ 2.0824 .

From Fig. 5b1, for the 10 μm long waveguide at a pulse width of 2.5fs, L_{NL} and L_D are calculated as 1.0792 μm and 5.8496 μm respectively with the characteristic propagation distance ($\approx 5L_D$) as 29.248 μm . In this case, the waveguide length $L = 10$ μm is much smaller compared to $5L_D$ resulting in only one clearly separated soliton peak in the temporal intensity despite the calculated soliton order(N) being ~ 2.3281 .

For the broadest Supercontinuum generated³¹ from Fig. 5c1 for the 1 mm long waveguide at a pulse width of 1fs, the L_{NL} and L_D are calculated as 2.1584 μm and 0.93594 μm with the characteristic propagation distance calculated as $\approx 5L_D = 4.6797$ μm . The waveguide length (L) of 1 mm for this design is much larger compared to the $5L_D$ resulting in a greater number of ejected solitons with distinct spectral peaks in the anomalous GVD regime that can be clearly identified as due to soliton fission³³. The extension of the spectral broadening to the long wavelengths is however due to the generation of red shifted waves formed by coupling of negative dispersion slope (in the vicinity of the second ZDW, the D slope is negative) with the anomalous GVD.

As the pulse width is less than 12fs for the generated SCs above, dispersive perturbation induces soliton fission and this can be modified in two ways. Primarily, as an ejected fundamental soliton shifts to longer wavelengths because of the Raman effect which is small in our case, the soliton encounters a varying value of β_2 , and its temporal width and peak power adjust themselves to conserve a unit soliton number during propagation. This effect is clearly seen in the broader Supercontinuum generated in Fig. 5c1,c2. The flatness of the spectrum is however achieved due to the low third order dispersion ($\beta_3 = 2.251048248652541 \times 10^{-3}$ ps^3/m) for this design at 1550 nm.

The second effect is due to the presence of higher-order dispersion which also leads to the transfer of energy from soliton to a narrow-band resonance in the normal GVD regime¹³. This is clearly seen in Fig. 5a1,b1 although the effect is quite small in SC generated in Fig. 5b1 (Fig. 5a2,b2 show their respective temporal evolution of

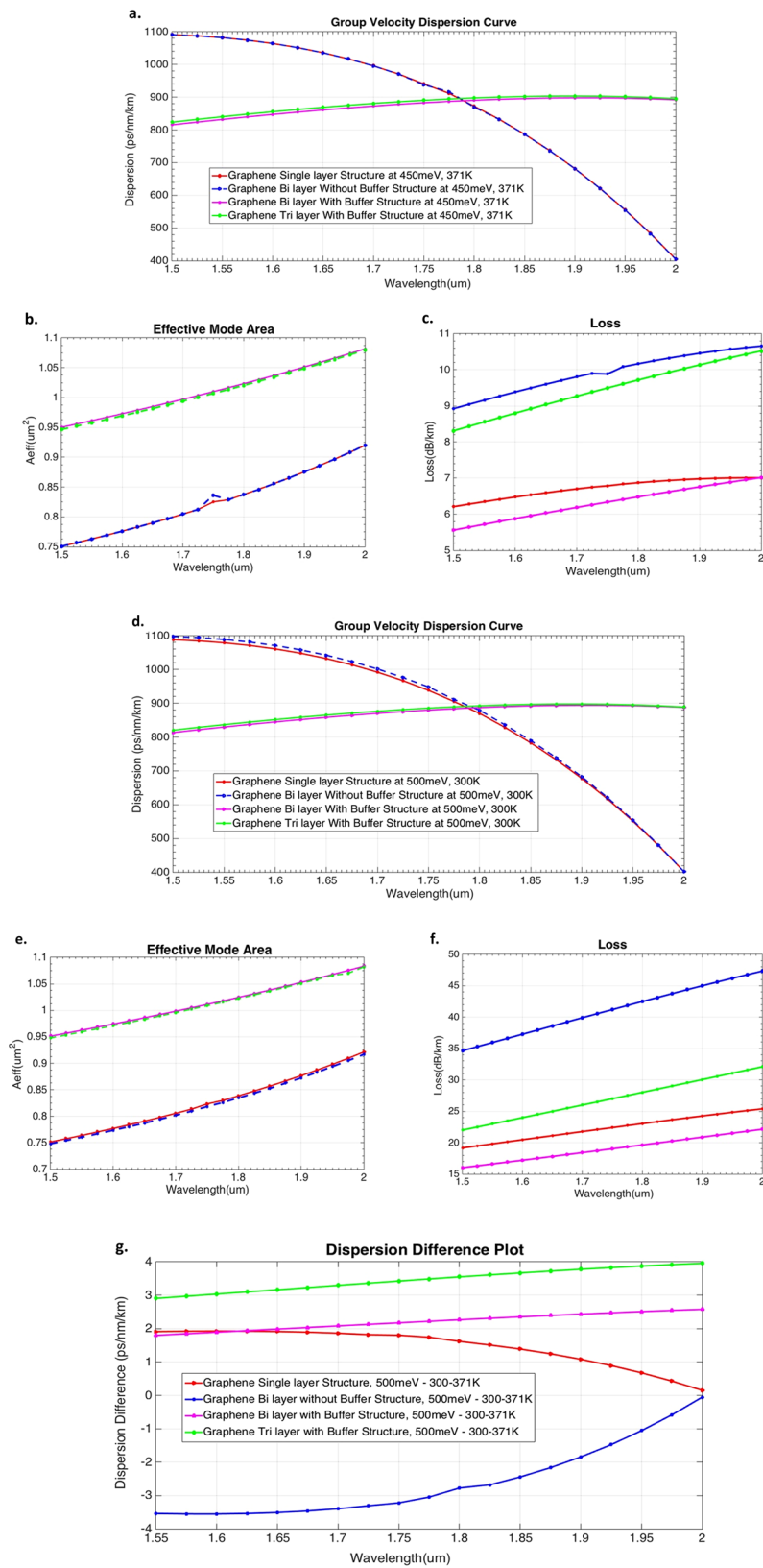


Figure 3. GVD, Effective mode Area and Loss plots for all the designed Graphene waveguides. (a–c) Calculated GVD curve, A_{eff} and loss of four different Graphene waveguides at 450 meV, 371 K. (d–f) Calculated GVD curve, A_{eff} and loss of four different Graphene waveguides at 500 meV, 300 K. (g) Difference between calculated GVDs at 500 meV, 300 K & 371 K.

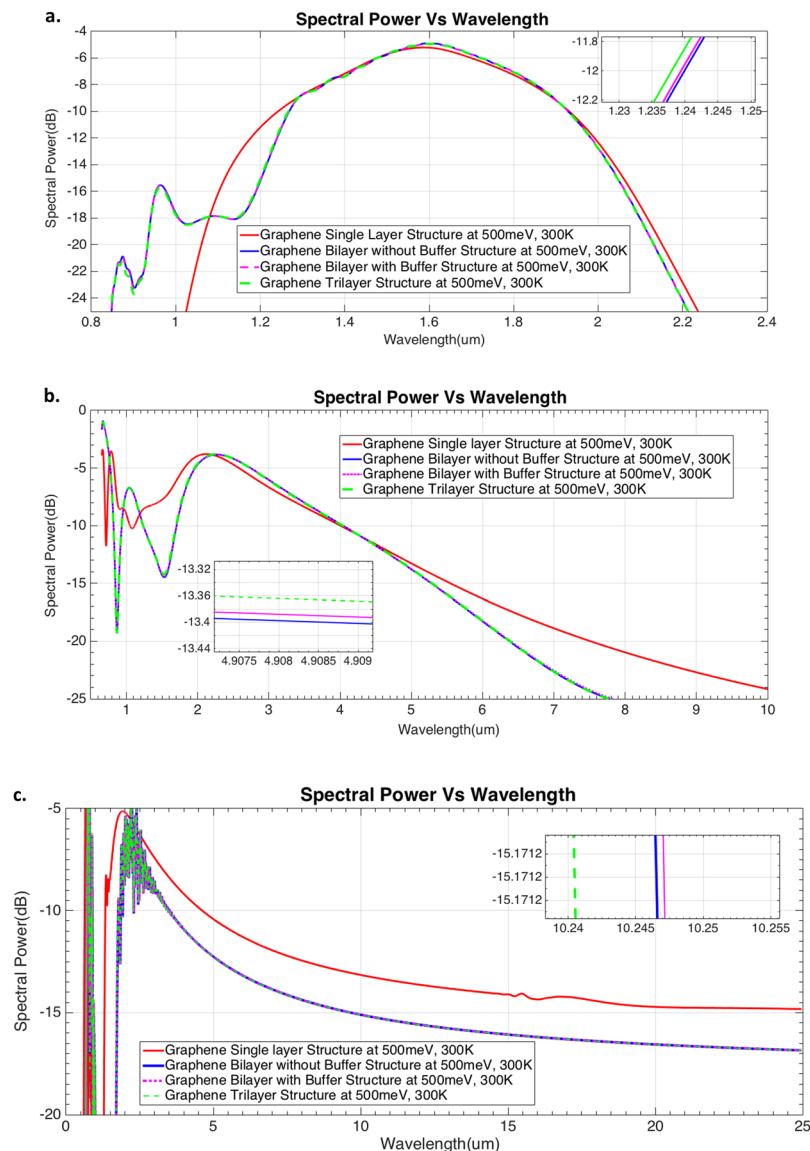


Figure 4. Supercontinuum generation in the designed Graphene waveguides. (a–c) Spectral Power plotted vs Wavelength for four designed Graphene waveguides at different peak input powers of 0.1W, 2W and 1W respectively (at a chemical potential of 500 meV, 300 K). Three different SC's were generated at these three input Powers, with varying parameters of pulse width and waveguide length. Zoomed plots in inset show the difference in Supercontinuum for each of the different structures at a given input power.

SC). However, this energy transfer decreases over the first few millimetres of propagation thereby limiting the non-linear spectral broadening^{34–36}.

These generated Supercontinua have many practical applications such as in DNA sensing, speed/pressure sensor monitoring and medical therapeutics as they cover the full functional band of lipids, proteins, genes, bacteria, viruses, chemicals and spectral region of most biomolecules^{37,38}. The selected Graphene bilayer with buffer structure can be tuned^{39,40} to 500 meV and practically fabricated by exfoliating graphene and defining its contacts around a particular flake using standard photolithography methods^{41–43}. An alternative method for this fabrication is to define the contacts first, transfer large area CVD Graphene on top, then add another layer of photoresist and use O₂ plasma to isolate devices^{44,45}.

From our results, an important observation is the behaviour of Graphene as a metal, and formation of SPPs on interaction with a dielectric at optical frequencies even without the negative real permittivity value of Graphene at 450 meV (300 K and 371 K temperature). This is different from the theory on Surface Plasmons^{46,47} which tells us that at a metal-dielectric interface, SPPs are formed when $\frac{k_2}{k_1} = -\frac{\epsilon_2}{\epsilon_1}$, where ϵ_1 and ϵ_2 are the permittivity of the metal and dielectric respectively. In our case, the permittivity of Graphene is not negative, however we still observe the formation of SPPs. This needs further analysis to confirm the behaviour of Graphene and could possibly open doors to a new understanding of Graphene and metals for new applications.

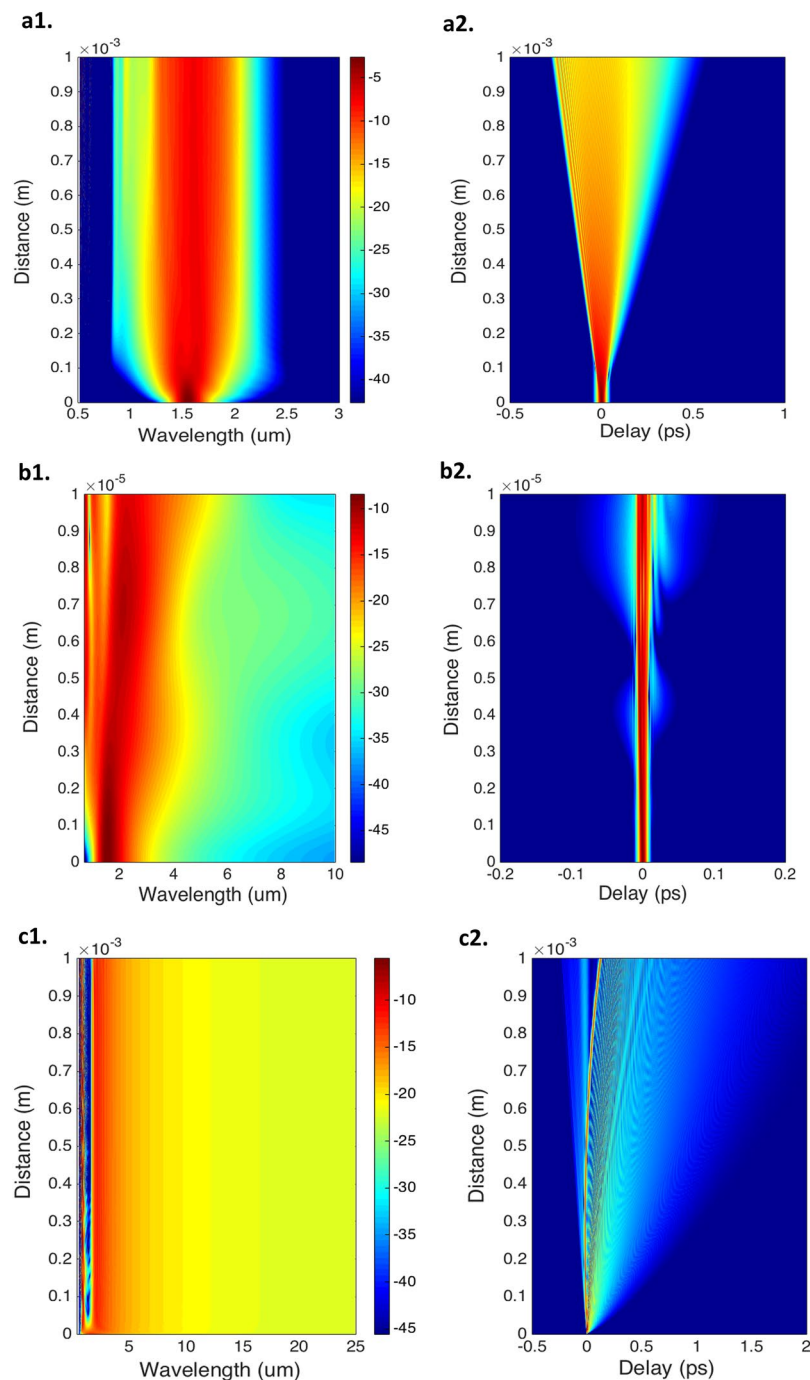


Figure 5. Calculated Spectral and Temporal evolution for the Graphene bi layer with buffer waveguide. **a1–c1**, Spectral and **a2–c2**, Temporal evolution of Supercontinuum for the designed Graphene bilayer with buffer waveguide (at 500meV, 300K) with pulse width of 10fs, 2.5fs and 1fs at three input peak powers of 0.1W, 2W and 1W respectively.

Conclusion

We have designed four waveguide structures using Graphene as the inner core, with Si_3N_4 of thickness - 0.6 μm and 0.8 μm for the outer core. This fundamentally tailored the plasmonic mode in the dielectric-metal-dielectric interface. With typical waveguide parameters, we achieved a large negative non-linear coefficient of $\gamma = -4.6330088494 \times 10^5$ 1/m-W due to negative non-linear Kerr coefficient of Graphene of the order, $n_2 = -1.1 \times 10^{-13}$ m^2/W that played a major role in stimulating a small Raman effect and thereby leading to broader Supercontinuum by the influence of solitons and dispersive waves.

We have shown that the Graphene Bilayer with Buffer waveguide (at 500 meV, 300 K) exhibits a SC extending from 1.5–25 μm at a very low input peak power of 1 W, with overall waveguide loss of only 16.5 dB/km. This is the broadest SC to the best of our knowledge.

Methods

The modal solutions in the designed Graphene waveguides were obtained using Full Vectorial H-field formulation with penalty term to eliminate the spurious solution. It is one of the most accurate and numerically efficient approaches to obtain the modal field profiles of a waveguide. Various quasi-TE and quasi-TM modes were calculated from equation (1),

$$\omega^2 = \frac{\iint [(\nabla \times H)^* \cdot \varepsilon^{-1}(\nabla \times H) + \left(\frac{\alpha}{\varepsilon}\right)(\nabla \cdot H)^*(\nabla \cdot H)] d\Omega}{\iint H^* \cdot \bar{\mu} H d\Omega} \quad (1)$$

from which the mode propagation constant $\beta(\omega)$ of the fundamental mode over a range of wavelengths was evaluated, and the effective index was calculated using equation (2),

$$N_{eff} = \frac{\beta(\omega)\lambda}{2\pi} \quad (2)$$

As chromatic dispersion of the waveguide manifests through the wavelength dependence of the refractive index $n(\lambda)$ (approximated by the refractive index equation, $n = \frac{c}{v}$, where c is the velocity of light in vacuum and v is the velocity of light in medium), the GVD parameter of the Graphene waveguide was calculated from the N_{eff} by equation (3),

$$D(\lambda) = \frac{d\beta_1}{d\omega} = -\frac{\lambda}{c} \frac{d^2 n_{eff}}{d\lambda^2} = -\frac{2\pi c}{\lambda^2} \beta_2 \left(\frac{ps}{nm \cdot km} \right) \quad (3)$$

Where $\beta_1 = \frac{1}{v_g}$, v_g is the group velocity of pulse envelop and the third-order dispersion (β_3) was calculated using equation (4),

$$\beta_3 = \frac{dD(\lambda)}{d\lambda} \left(\frac{ps^3}{m} \right) \quad (4)$$

The GVD (Group velocity Dispersion), TOD (Third order Dispersion) and subsequently other higher-order dispersion coefficients were calculated from N_{eff} . This calculation was written as a MATLAB code and benchmarked with the material dispersion of Silicon to test its accuracy.

For SCG, the Generalized Non-Linear Schrödinger Equation (GNLSE) was solved using the Split-step Fourier method using equation (5),

$$\frac{\partial A}{\partial z} + \frac{\alpha}{2} A - \sum_{k \geq 2} \frac{i^{k+1}}{k!} \beta_k \frac{\partial^k A}{\partial T^k} = i\gamma \left(1 + i\tau_{shock} \frac{\partial}{\partial T} \right) \left(A(z, t) \int_{-\infty}^{+\infty} R(T') \times |A(z, T - T')|^2 dT' + i\gamma_R(z, T) \right) \quad (5)$$

The left side of the equation (5) models the linear propagation effects while the right side models the non-linear effects. This code was incorporated from Dudley *et al.*⁴⁸, moderated and tested for accuracy and efficiency with experimental studies. The non-linear coefficient (γ) in equation (5) is calculated using equation (6),

$$\gamma = \frac{2\pi n_2}{\lambda_0 A_{eff}} \quad (6)$$

where n_2 is the non-linear Kerr coefficient, λ_0 is the pump wavelength and A_{eff} is the effective mode area.

The results of FEM have been benchmarked⁴⁹ as well with the experimental analysis of other metals to confirm the behaviour of Graphene as a metal at 450 meV (300 K and 371 K).

References

1. Alfano, R. R. *The Supercontinuum laser source*. (Springer-Verlag, 1989).
2. Leon-Saval, S. G., Birks, T. A., Wadsworth, W. J., Russell, P. S. & Mason, M. W. Supercontinuum generation in submicron fibre waveguides. *Optics Express* **12**, 2864 (2004).
3. Yu, Y. *et al.* 1.8–10 μm mid-infrared supercontinuum generated in a step-index chalcogenide fiber using low peak pump power. *Optics Letters* **40**, 1081 (2015).
4. Sharma, M. & Konar, S. Three octave spanning supercontinuum by red-shifted dispersive wave in photonic crystal fibers. *Journal of Modern Optics* **63**, 501–510 (2015).
5. Cheng, T. *et al.* Mid-infrared supercontinuum generation spanning 2.0 to 15.1 μm in a chalcogenide step-index fiber. *Optics Letters* **41**, 2117 (2016).
6. Fung, M. *et al.* A higher power and high efficiency supercontinuum generated by small core UHNA3 fiber. *15th International Conference on Optical Communications and Networks (ICOON)*, doi:10.1109/icoon.2016.7875875 (2016).
7. Cheng, T. *et al.* Experimental investigation of mid-infrared supercontinuum generation in chalcogenide step-index optical fibers. *Proc. SPIE, Nonlinear Frequency Generation and Conversion: Materials and Devices XVI* **10088**, 100880B, doi:10.1117/12.2255680 (2017).
8. Smektala, F. *et al.* Nonlinear glasses-based microstructured or step-index optical fibers: mid-IR supercontinuum generation and IR spectroscopy applications. *Proc. SPIE, Optical Components and Materials XIV* **10100**, 1010012, doi:10.1117/12.2257044 (2017).
9. Zhang, B. *et al.* High Brightness 2.2–12 μm Mid-Infrared Supercontinuum Generation in a Nontoxic Chalcogenide Step-Index Fiber. *Journal of the American Ceramic Society* **99**, 8, 2565 (2016).

10. Jain, D. *et al.* High power, ultra-broadband supercontinuum source based on highly GeO₂ doped silica fiber. *Proc. SPIE, Fiber Lasers XIV: Technology and Systems* **10083**, 1008318, doi:10.1117/12.2251648 (2017).
11. Yao, J. *et al.* High-mode mid-infrared supercontinuum source based on low-loss fusion spliced silica and chalcogenide fiber. *15th International Conference on Optical Communications and Networks (ICOON)*, doi:10.1109/icoon.2016.7875631 (2016).
12. Yang, L. *et al.* 2.03–2.80 μm supercontinuum generation in an all-fiberized holmium-doped ZBLAN fiber amplifier. *15th International Conference on Optical Communications and Networks (ICOON)*, doi:10.1109/icoon.2016.7875767 (2016).
13. Xu, Q., Zhao, Y., Wang, M., Zhang, Y. & Hao, B. Supercontinuum generation in highly nonlinear low-dispersion photonic crystal fiber. *Proc. SPIE, International Conference on Optical and Photonics Engineering (icOPEN 2016)* **10250**, 102500E, doi:10.1117/12.2266695 (2017).
14. Azaizia, S., Balocchi, A. and Lagarde, D. Physics and Simulation of Optoelectronic Devices XXV. *SPIE Photonics West OPTO* <https://spie.org/Documents/ConferencesExhibitions/PW170-Abstracts-lr.pdf#page=3> (2017).
15. Day, C. Andre Geim and Konstantin Novoselov win 2010 physics Nobel for graphene. *Physics Today*. doi:10.1063/pt.4.0866 (2010).
16. Kim, Y. D. *et al.* Bright visible light emission from graphene. *Nature Nanotechnology* **10**, 676–681 (2015).
17. Novoselov, K. S. *et al.* A roadmap for graphene. *Nature* **490**, 192–200 (2012).
18. Dremetsika, E. *et al.* Measuring the nonlinear refractive index of graphene using the optical Kerr effect method. *Optics Letters* **41**, 3281 (2016).
19. Rahman B. M. A. and Agrawal A. *Finite Element Modelling for Photonics*. (Artech House, 2013).
20. Rahman, B. M. A. Finite element analysis of optical waveguides. *Progress In Electromagnetics Research* **10**, 187–216 (1995).
21. Lin, I. T. Optical properties of graphene from the THz to the visible spectral region, PhD thesis, University of California, Los Angeles (2012).
22. Gusynin, V. P., Sharapov, S. G. & Carbotte, J. P. Magneto-optical conductivity in graphene. *Journal of Physics: Condensed Matter* **19**, 026222 (2006).
23. Xu, H. J., Lu, W. B., Zhu, W., Dong, Z. G. & Cui, T. J. Efficient manipulation of surface plasmon polariton waves in graphene. *Applied Physics Letters* **100**, 243110 (2012).
24. Vakil, A. & Engheta, N. Fourier optics on graphene. *Physical Review B* **85** (2012).
25. He, S., Zhang, X. & He, Y. Graphene nano-ribbon waveguides. *arXiv preprint:1305.6500* <https://arxiv.org/abs/1305.6500> (2013).
26. Anker, J. N. *et al.* Biosensing with plasmonic nanosensors. *Nature Materials* **7**, 442–453 (2008).
27. Ashok, N., Lee, Y. L. & Shin, W. Chalcogenide waveguide structure for dispersion in mid-infrared wavelength. *Japanese Journal of Applied Physics* **56**, 032501 (2017).
28. Ahmed, S. F. U., Nayemuzzaman, S. & Faisal, M. Ultra-high nonlinear photonic crystal fiber with GeO₂ doped core. *2016 9th International Conference on Electrical and Computer Engineering (ICECE)*, doi:10.1109/icece.2016.7853963 (2016).
29. Li, N. *et al.* Coherent supercontinuum generation from 1.4 to 4 μm in a tapered fluorotellurite microstructured fiber pumped by a 1980 nm femtosecond fiber laser. *Applied Physics Letters* **110**, 061102 (2017).
30. Siwach, P., Kumar, A. & Saini, T. S. Supercontinuum Generation in Ge 11.5 As 24 Se 64.5 based Chalcogenide Few-Mode Fiber. *13th International Conference on Fiber Optics and Photonics*, doi:10.1364/photronics.2016.w3a.69 (2016).
31. Dudley, J. M., Genty, G. & Coen, S. Supercontinuum generation in photonic crystal fiber. *Reviews of Modern Physics* **78**, 1135–1184 (2006).
32. Genty, G. Supercontinuum generation in optical fibers: 40 years of nonlinear optics in one experiment. *Photonics@be Doctoral School* http://www.telecom.fpms.ac.be/PhotonDoctoralSchool2013/Documents/Genty_Supercontinuum.pdf (2013).
33. Yin, L., Lin, Q. & Agrawal, G. P. Soliton fission and supercontinuum generation in silicon waveguides. *Optics Letters* **32**, 391 (2007).
34. Indra, L. *et al.* Picosecond pulse generated supercontinuum as a stable seed for OPCPA. *Optics Letters* **42**, 843 (2017).
35. Epping, J. P. *et al.* On-chip visible-to-infrared supercontinuum generation with more than 495 THz spectral bandwidth. *Optics Express* **23**, 19596 (2015).
36. Jiang, X. *et al.* Deep-ultraviolet to mid-infrared supercontinuum generated in solid-core ZBLAN photonic crystal fibre. *Nature Photonics* **9**, 133–139 (2015).
37. Singhal, A. & Shaham, S. Infrared laser-induced gene expression for tracking development and function of single *C. elegans* embryonic neurons. *Nature Communications* **8**, 14100 (2017).
38. Barth, A. Infrared spectroscopy of proteins. *Biochimica et Biophysica Acta (BBA) - Bioenergetics* **1767**, 1073–1101 (2007).
39. Yu, Y. J. *et al.* Tuning the Graphene Work Function by Electric Field Effect. *Nano Letters* **9**, 3430–3434 (2009).
40. Zhang, Y. *et al.* Direct observation of a widely tunable bandgap in bilayer graphene. *Nature* **459**, 820–823 (2009).
41. Wei, D. & Liu, Y. Controllable Synthesis of Graphene and Its Applications. *Advanced Materials* **22**, 3225–3241 (2010).
42. Liu, L. *et al.* Nanosphere Lithography for the Fabrication of Ultranarrow Graphene Nanoribbons and On-Chip Bandgap Tuning of Graphene. *Advanced Materials* **23**, 1246–1251 (2011).
43. Wang, X. & Shi, Y. Fabrication Techniques of Graphene Nanostructures. *Nanofabrication and its Application in Renewable Energy*, 1–30, doi:10.1039/9781782623380-00001 (The Royal Society of Chemistry, 2014).
44. Aliofkhaeaei, M. *et al.* *Graphene science handbook: Fabrication Methods*. (CRC Press, Taylor & Francis Group, 2016).
45. Li, B. *et al.* Deep UV hardening of photoresist for shaping of graphene and lift-off fabrication of back-gated field effect biosensors by ion-milling and sputter deposition. *Carbon* **118**, 43–49 (2017).
46. Maier, S. A. Surface Plasmon Polaritons at Metal / Insulator Interfaces. *Plasmonics: Fundamentals and Applications*, 21–37, doi:10.1007/0-387-37825-1_2 (Springer US, 2007).
47. Wang, X. *et al.* Excitation and propagation of surface plasmon polaritons on a non-structured surface with a permittivity gradient. *Light: Science & Applications* **5** (2016).
48. Dudley, J. M. & Taylor, J. R. *Supercontinuum generation in optical fibers*. (Cambridge University Press, 2010).
49. Veronis, G. & Fan, S. Modes of Subwavelength Plasmonic Slot Waveguides. *Journal of Lightwave Technology* **25**, 2511–2521 (2007).
50. Hanson, G. W. Dyadic Green's functions and guided surface waves for a surface conductivity model of graphene. *Journal of Applied Physics* **103**, 064302 (2008).

Acknowledgements

S.S.B. acknowledges the support of City, University of London for Tuition fee waiver scholarship.

Author Contributions

S.S.B. designed the waveguides, numerical analysis, performed theoretical analysis and executed the research. A.A. supervised the research and designed the methodology. S.S.B. wrote the paper and A.A. gave the input and contributed to discussions and shaping of the manuscript.

Additional Information

Competing Interests: The authors declare that they have no competing interests.

Publisher's note: Springer Nature remains neutral with regard to jurisdictional claims in published maps and institutional affiliations.



Open Access This article is licensed under a Creative Commons Attribution 4.0 International License, which permits use, sharing, adaptation, distribution and reproduction in any medium or format, as long as you give appropriate credit to the original author(s) and the source, provide a link to the Creative Commons license, and indicate if changes were made. The images or other third party material in this article are included in the article's Creative Commons license, unless indicated otherwise in a credit line to the material. If material is not included in the article's Creative Commons license and your intended use is not permitted by statutory regulation or exceeds the permitted use, you will need to obtain permission directly from the copyright holder. To view a copy of this license, visit <http://creativecommons.org/licenses/by/4.0/>.

© The Author(s) 2017